Phytoplankton dynamics driven by vertical nutrient fluxes during the spring inter-monsoon period in the northeastern South China Sea

Qian P. Li*, Yuan Dong, Yanjun Wang

South China Sea Institute of Oceanology, Chinese Academy of Sciences, Guangzhou, China

Submitted to Biogeosciences on March 27, 2015

Revised July 29, 2015

*Correspondence to: qianli@scsio.ac.cn

Abstract

A field survey from the coastal ocean zones to the offshore pelagic zones of the northeastern South China Sea (SCS) was conducted during the inter-monsoon period of May 2014 when the region was characterized by prevailing low-nutrient conditions. Comprehensive field measurements were made for not only hydrographic and biogeochemical properties but also phytoplankton growth and microzooplankton grazing rates. We also performed estimations of the vertical turbulent diffusivity and diffusive nutrient fluxes using a Thorpe-scale method and the upwelling nutrient fluxes by Ekman pumping using satellite-derived wind stress curl. Our results suggest that phytoplankton chlorophyll patchiness in the northeastern SCS during the study period could be largely controlled by vertical nutrient fluxes with combined contributions from both turbulent diffusion and curl-driven upwelling. Our results also reveal the generally increasing role of turbulent diffusion but decreasing role of curl-driven upwelling on vertical transport of nutrients from the coastal ocean zones to the offshore pelagic zones in the northeastern SCS. Elevated nutrient fluxes observed near Dongsha Island were found to support high new production leading to net growth of a diatom-rich phytoplankton community, whereas the low nutrient fluxes near southwest Taiwan resulted in a negative net community growth leading to a decline of a picoplankton-dominant phytoplankton bloom.

1. **Introduction**

Nutrient fluxes from below the euphotic zone are essential for phytoplankton primary production in the surface ocean (Eppley and Peterson, 1979), while the mechanisms regulating those fluxes are still inadequately understood in the northern South China Sea (SCS), one of the largest margin seas in the world, particularly during the spring intermonsoon period. Wind-driven coastal upwelling, river discharges, and inter-shelf nutrient transport are important mechanisms supplying nutrients to the euphotic zone of the northern SCS (Liu et al., 2002; Gan et al., 2010; Han et al., 2013), while their contributions to primary production are mostly limited to coastal regions as these nutrients will be utilized in the coastal waters before reaching the large area of the northeastern SCS. Kuroshio intrusion will dilute the northern SCS waters with the low nutrient North Pacific waters (Farris and Wimbush. 1996), which appears to be much weaker during April-September (Centurioni et al., 2004). Contribution of nitrogen fixation to new production of the northern SCS is generally negligible compared to the nitrate-based new production (Chen et al., 2005; Bombar et al., 2010). Atmospheric deposition of anthropogenic nitrogen could support up to ~20% of the annual new production in the northern SCS exceeding those from riverine inputs (Kim et al., 2014). But its contribution would be much less during the spring inter-monsoon season as the reduced rate of atmospheric deposition (Lin et al., 2009).

Diapycnal mixing by turbulent dissipation was recently found to be important for the supply of new nitrogen in the northern SCS, where the vertical turbulent diffusivities could be an order of magnitude higher than the adjacent West Pacific Ocean (Tian et al., 2009; Liu and Lozovatsky 2012; Yang et al., 2014). It was also suggested that phytoplankton blooms off the west coast of the northern SCS could be induced by wind stress curl-driven upwelling during the spring inter-monsoon season (Wang and Tang 2014), which would cause a local uplift of isopycnals leading to nutrient injection into the euphotic zone with subsequent changes of community structure and productivity (Rykaczewski and Checkley 2008). By modifying the surface wind stress and wind stress curl via air-sea coupling, eddy-induced Ekman pumping (Gaube et al., 2013) are important for phytoplankton production in the northern SCS during the inter-monsoon transition period (Lin et al., 2010). As both intermittent turbulent diffusion and

63 wind-driven Ekman pumping influencing the vertical transport of nutrients on temporal
64 scales similar to the generation time of phytoplankton, they would thus have large
65 impacts on the plankton dynamics of the upper ocean (Cullen et al., 2002). It is therefore
66 important to investigate the roles of these two mechanisms in driving the variability of
67 phytoplankton biomass and primary production in the large area of the northern SCS.
68 Spatial distribution of phytoplankton at sea is a result of complex interactions
69 between physical and biological processes (Davis et al., 1991; Abraham 1998). In
70 addition to the vertical nutrient fluxes, phytoplankton biomass and productivity of the
71 northern SCS were influenced by growth-grazing dynamics (Chen 2005; Huang et al.,
72 2011; Zhou et al., 2011; Chen et al., 2013). Shifts in the dominance of phytoplankton
73 species in the western SCS were believed to be driven by a close coupling of the
74 mortality rates of different phytoplankton groups via common grazers such as
75 nanoflagellates (Chen et al., 2009). There was on average ~61% of phytoplankton growth
76 lost to microzooplankton grazing in coastal upwelling regions of the northern SCS in
77 response to increased nutrient fluxes, whereas growth and grazing mortality rates were
78 mostly balanced on the shelf and shelf break areas without upwelling events (Huang et al.,
79 2011). It was also suggested that the balance of phytoplankton growth and
80 microzooplankton grazing in the pelagic northern SCS could be perturbed by physical
81 disturbances such as eddies, fronts, and typhoons, leading to large deviations of
82 planktonic ecosystem from the steady state (Zhou et al., 2011; Chen et al., 2013).
83 Here, we present results of a field survey from the coastal ocean zones to the offshore
84 pelagic zones in the northeastern SCS conducted during the spring inter-monsoon
85 transition of May 2014, when the region was characterized by prevailing low nutrient
86 conditions as a result of weak and variable winds (Lin et al., 2010). Comprehensive
87 measurements were made for hydrographic and biogeochemical properties, as well as
88 biological rates including phytoplankton growth and grazing rates and net nutrient
89 consumption rates. We also performed estimations of the vertical turbulent diffusivity
90 and diffusive nutrient fluxes using a Thorpe-scale method (Gargett and Garner 2008; Li
91 et al., 2012) and the upwelling nutrient fluxes by Ekman pumping using satellite-derived
92 wind stress curl (Gill 1982; Risien and Chelton 2008). In synthesizing these field data,
93 the focus of this paper are to (1) investigate the spatial patterns of vertical nutrient fluxes

in the northeastern SCS, (2) determine the relative roles of turbulent diffusion and Ekman pumping to vertical transport of nutrients in the upper ocean, and (3) understand the linkage between vertical nutrient fluxes and phytoplankton dynamics in the northeastern SCS during the spring inter-monsoon period.

2. Materials and methods

2.1.Site description, field sampling, and measurements

The northern South China Sea is influenced by river discharge, seasonal monsoons, upwelling, mixing, internal waves and eddies. There are typically high nutrients in the coastal regions of the northern SCS due to river discharge and inter-shelf transport, as well as upwelling/mixing (Gan et al., 2010), in contrast to the oligotrophic low-latitude offshore regions with strong stratification. The northern SCS is also influenced by the penetration of the Kuroshio Current through the Luzon Strait, which is a northward flowing oligotrophic current along the east coast of the Philippines (Farris and Wimbush 1996). The penetrated Kuroshio waters with high temperature and salinity but extremely low nutrients are transported westward via eddies and Ekman advection (Centurioni et al., 2004) influencing a large area of the northern SCS on seasonal and annual time-scales.

A field survey of the northeastern SCS (Fig. 1) was conducted during May 2014 aboard the *R/V Shiyan III* of the South China Sea Institute of Oceanology. From May 14th to May 16th, 2014, a transect from the coastal ocean zone near Shantou to the offshore pelagic zone near the Luzon Strait was comprehensively sampled to investigate the spatial patterns of hydrographic and biogeochemical properties in the region. One station (S_1 of 22°N, 119.5°E) served as a time-series reference station with continuous CTD sampling including 13 casts within 24 hours (start: 10:00 am, May 18th, 2014). Two stations with one located near the southwest of Taiwan (Station A: 21.9°N, 120°E with a bottom depth of 1547 m) and the other in the southeast of Dongsha Island (Station B: 20.5°N, 117°E with a bottom depth of 607 m) were selected for dilution experiments to quantify phytoplankton growth and microzooplankton grazing rates, which will be further described in next few sections.

For each station, discrete seawater samples at depths of 0 m, 25 m, 50 m, 75 m, 100 m, 200 m, 300 m, 500 m, and 700 m were collected using a SeaBird SBE 9/11 CTD rosette

water sampler system, which also provides high resolution hydrographic measurements of the upper water column with internal pressure, conductivity, and temperature sensors. After inline filtrations from the PVC Niskin bottles through 0.8 μm Nuclepore filters, seawater samples for nutrients were frozen immediately and stored in a refrigerator until final analyses after the cruise. For chlorophyll-*a* sampling, 500 ml of seawater was gently filtered (<50 mmHg) through a GF/F (Whatman) filter, which was wrapped in a piece of aluminum foil and kept at -20°C on board. Upon return to the lab, chlorophyll-*a* samples were sonicated for 20 min and extracted in 5 ml 90% acetone at 4°C in the dark for 24 hours. These samples were centrifuged at 4000 rpm for 10 min before final determinations by standard fluorescence methods (Parsons et al., 1984) using a Turner Designs Model 10 Fluorometer. Concentrations of nitrate plus nitrite (NO_3+NO_2), phosphate (PO_4) and silicate (SiO_4) were determined by standard colorimetric methods (Li and Hansell 2008) using a Seal AA3 auto analyzer (Bran-Lube, GmbH).

2.2. Remote sensing observations

High-resolution satellite observations, including sea surface temperature (SST), sea surface chlorophyll (SSChl), surface geostrophic currents, as well as surface wind stresses and Ekman upwelling velocities, were used to assess the surface distributions of hydrographic and biogeochemical properties in the northern SCS during the period of the survey. Monthly averaged sea surface chlorophyll-*a* ($0.04^\circ \times 0.04^\circ$) was acquired from the NASA's Moderate Resolution Imaging Spectroradiometer data observed by the Aqua Satellite (MODIS-Aqua). Near real time geostrophic currents ($0.2^\circ \times 0.2^\circ$) were from the NOAA's CoastWatch data based on the daily sea level height anomaly and a climatological mean dynamic height field by NOAA/AOML. Daily sea surface temperature ($0.1^\circ \times 0.1^\circ$) was acquired from the NOAA's Geostationary Operational Environmental Satellite –Polar Operational Environmental Satellite program (GOES-POES). Daily Ekman upwelling velocities and surface wind stresses with a resolution of $0.25^\circ \times 0.25^\circ$ were derived from the Advanced Scatterometer data by the European Meteorological and Operational satellite program (METOP-ASCAT). The Ekman pumping velocity (w_e, negative for downwelling) at the depth of Ekman layer is calculated as (Gill, 1982)

$$w_e = \frac{1}{\rho_w}\left(\nabla \times \frac{\tau}{f}\right) \quad (1)$$

where ρ_w is the density of seawater, which is assumed constant at 1024 kg m^{-3}; f is the Coriolis parameter; τ is the vector of wind stress.

2.3 Thorpe-scale analyses and vertical diffusivity

We applied a Thorpe-scale based approach (Thorpe 1977; Galbraith and Kelley 1996; Gargett and Garner 2008; Li et al., 2012) to estimate fine structure and turbulent diffusivity for each station using CTD downcast data. The method combined several criteria to determine the real overturns from a density profile (Li et al., 2012), including the test of minimum thickness, the run-length and water mass tests (Galbraith and Kelley 1996), as well as the tests of minimal overturn ratio and maximal T/S tightness (Gargett and Garner 2008). These criteria ensure that the maximal density difference within an overturn is greater than twice the measurement noise (0.001 kg m^{-3}). The length scale of an overturn is larger than twice the vertical resolution (Nyquist theorem) and larger than a minimum thickness (Galbraith and Kelley 1996). The percentage of positive/negative displacements within an overturn (the overturn ratio) is larger than 0.2 and the deviations on a T/S diagram are less than 0.003 (Gargett and Garner 2008). The vertical resolution of CTD sampling during the cruise was ~10 cm with a fall rate of ~2.4 m s^{-1}. Therefore, only overturns larger than 0.5 m are included, to obtain five data point resolution. Data from the upper 10 m were discard, as the Thorpe approach is not strictly valid there. Once an overturn is identified, the Thorpe scale (L_T) is calculated from the root mean square of the vertical displacement (d_z) as $L_T = (\Sigma d_z^2)^{0.5}$.

Turbulent kinetic energy dissipation rate (ε) is calculated from L_T and N by

$$\varepsilon = 0.64 \cdot L_T^2 \cdot N^3 \quad (2)$$

where N is the buoyancy frequency given by $N^2 = -g\rho_0^{-1}(\partial\rho/\partial z)$ with g the gravitational acceleration, ρ_0 the mean density, and $\partial\rho/\partial z$ the density gradient across each overturn (Galbraith and Kelley 1996). According to Osborn (1980), the vertical diffusivity (K_z) can

185 be estimated from ε and N by

186 $$K_z = 0.2 \cdot \varepsilon \cdot N^{-2}$$

187 (3)

188 The diffusive nutrient fluxes at the depth of interest can be estimated by multiplying the
189 diffusivity (K_z) by the local nutrient gradient ($\partial C/\partial z$).

190

191 2.4 Setup of dilution experiments

192 Phytoplankton growth and microzooplankton grazing in the surface waters of stations
193 A and B near the edge of continental shelf (Fig. 1) were assessed on board using dilution
194 technique (Landry and Hassett 1982; Landry et al., 1998; Li et al., 2011) on May 13th and
195 May 17th, 2014. All the bottles, tubing and carboys were soaked in 10% (v/v)
196 hydrochloric acid solution for over 24 hours and they were rinsed several times with
197 deionized water and seawater before each experiment. Surface seawater, collected by an
198 acid-washed polyethylene bucket, was screened through a 200-μm mesh before being
199 transferred into polycarbonate carboys as raw seawater. A dilution series was prepared
200 with 0%, 25%, 50%, 75%, and 100% unfiltered seawater in duplicated polycarbonate
201 bottles. Measured amounts of particle-free seawater, obtained by filtering the raw
202 seawater with 0.45 μm filters, were added to 2.4-liter polycarbonate bottles. These
203 samples were then enriched with additional nutrients to promote constant growth of
204 phytoplankton. Finally, each bottle was gently filled with unfiltered seawater to its
205 capacity. There was also one bottle filled with 100% unfiltered raw seawater without
206 nutrient enrichment to serve as the control for our experiment. All the bottles were tightly
207 capped and incubated for 24 hours in a deck incubator, which was covered with a neutral
208 density screen to mimic the natural sunlight and filled with flowing seawater from the sea
209 surface to control the temperature. Duplicate 300 ml samples were taken from each bottle
210 before and after the dilution experiments for chlorophyll-*a* measurements.

211 Specific rates of nutrient-saturated phytoplankton growth (μ_n, d^{-1}) and
212 microzooplankton grazing (g, d^{-1}) are estimated by least-square regression between the
213 net growth rates (η, d^{-1}) and the dilution factors (D) as

$$\eta = \frac{1}{t}\ln\left(\frac{P_t}{P_0}\right) = \mu_n - D \cdot g \quad (4)$$

where P_0 and P_t are the initial and final concentrations of chlorophyll-*a*, respectively and *t* is the duration of the incubation. The natural phytoplankton growth rate (μ), which is often subjected to nutrient limitation (Landry et al., 1998), is finally estimated from the net growth rate of raw seawater without nutrient enrichment (η_{raw}) by $\mu=\eta_{raw}+g$.

To examine the response of the phytoplankton community to nutrient enrichment, two bottles of raw seawater with nutrient additions were incubated for 4 days, with chlorophyll-*a* and nutrient samples taken at the very beginning and each day afterwards. Nutrient data within the exponential growth phase was used to estimate the specific net nutrient consumption rate (*m*) of the incubated community by linear regression of *ln*(*C*) and *t* assuming

$$\frac{dC}{dt} = -m \cdot C \quad (5)$$

where *C* is the concentration of dissolved nutrients in the sample.

3. Results

3.1 Hydrographic dynamics of the northeastern South China Sea

Based on satellite data and field observations during the survey of May 2014, three regions could be distinguished in the northeastern SCS (Fig. 1): the coastal ocean zone (stations $C_{1\text{-}6}$), the offshore pelagic zone (stations $C_{7\text{-}10}$), and the water-intrusion zone near the Luzon Strait (stations $C_{11\text{-}13}$). These three different zones are influenced by a diverse set of physical processes. The coastal ocean zone, which could be further separated into two different subregions including the near-shore area (stations $C_{1\text{-}2}$) and the continental shelf (stations $C_{3\text{-}6}$), was strongly influenced by wind-driven upwelling processes including Ekman transport and Ekman pumping (Gan et al., 2010). The near-shore area was characterized by extremely low sea surface temperature (Fig. 2a) as a result of deep, cold water upwelled via Ekman transport driven by southwest monsoon along the shore, while Ekman pumping induced by wind stress curl showed a significant

increase near the edge of the continental shelf far away from the coastline (Fig. 2b). Upward transport of the deeper water with lower temperature but higher salinity along the sharp shelf ridge was clearly observed during the survey (Fig. 3a and 3b), which could be a result of direct upwelling or alongshore advection of upwelled waters from upstream. Both the offshore pelagic zone and the water-intrusion zone were far from the coast with bottom depths more than 2000 m (Fig. 1). The offshore pelagic zone was relatively stable with weak surface geostrophic currents, while the water-intrusion zone was strongly influenced by intrusion of the Kuroshio Current into the SCS through the Luzon Strait.

Sea surface temperature from satellite remote sensing showed a generally increasing trend from the coastal regions near Shantou to the offshore regions near Luzon Strait due to the decreasing latitude (Fig. 2a). Substantial differences of surface temperature were also observed during the survey, with an average of 24.0 ± 0.6 $^{\circ}$C near the coast, 25.2 ± 0.2 $^{\circ}$C on the continental shelf, 28.4 ± 0.5 $^{\circ}$C in the offshore pelagic zone, and 29.1 ± 0.5 $^{\circ}$C near the Luzon Strait (Fig. 3a). The observed cross-shelf gradient of surface temperature from the discrete bottle samples was in good agreement with the satellite SST image. Surface salinity was less variable than temperature from near-shore to offshore with a difference of less than 0.3 during the survey (Fig. 3b). Surface salinity was on average 33.9 ± 0.2 in the near-shore area and increased slightly to 34.1 ± 0.1 on the continental shelf. Though the surface salinity between the offshore pelagic zone (33.8 ± 0.1) and the water-intrusion zone (33.9 ± 0.3) differed only slightly, substantially higher subsurface salinities were observed in the latter one (Fig. 3b), possibly resulting from Kuroshio intrusions that carried higher temperature and salinity North Pacific waters into the South China Sea through the Luzon Strait (Chao et al., 1996).

As suggested by the satellite geostrophic current data during the survey (vectors of Fig. 2a), there were anticyclonic and cyclonic eddies found in the southwest and the southeast of the Dongsha Island, respectively. Station B was located at the edge of these two mesoscale eddies, with strong southward-flowing surface geostrophic currents from the eddy-eddy interactions. These could lead to increased vertical mixing in the upper water column (Mahadevan and Tandon 2006). Prevailing wind stresses in the northeastern SCS were generally southwest during the study period except two regions where wind stress changed direction (vectors of Fig. 2b): one in the northwest of

Dongsha Island with southerly winds and the other in the Luzon Strait with westerly winds. The magnitude of upwelling/downwelling velocity by Ekman pumping was generally less than 10^{-5} m s^{-1} during our study (Fig. 2b). There was sporadic curl-driven upwelling observed in several places of the offshore pelagic zone and the water-intrusion zone, though these regions were predominantly downwelling. Strong curl-driven upwelling (>0.5×10^{-5} m s^{-1}) was only found near the edge of the continental shelf over abrupt changes of bathymetry. There were temporal variability of Ekman pumping found during the spring intermonsoon period in both coastal (C_6) and offshore (C_{13}) regions (Fig. 2d). Ekman velocities during our sampling duration of May 14th-16th, 2015 were relatively low but representative of the entire spring intermonsoon period from May 8th to June 7th, 2014 with substantially low wind intensity (Fig. 2d).

3.2 Spatial patterns of chlorophyll-*a* and nutrients in the northeastern South China Sea

Sea surface chlorophyll-*a* in the northeastern SCS during May 2014 was very high in the coastal ocean zone – particularly in the near-shore regions – and decreased slightly on the continental shelf (Fig. 2c). In contrast, there was generally low sea surface chlorophyll-*a* in the large areas of the offshore pelagic zone and the water-intrusion zone. The measured surface chlorophyll-*a* from discrete samples during our survey (Fig. 3c), varying from 0.04 to 0.92 μg L^{-1}, were in good agreement with the satellite remote sensing data. In particular, surface chlorophyll-*a* along the section showed a general seaward-decreasing trend from the costal regions of 0.72 ± 0.36 μg L^{-1} to the offshore regions of 0.09 ± 0.04 μg L^{-1}, which was consistent with the decrease of surface nitrate concentrations from >1.0 μmol L^{-1} near coast to <1.0 μmol L^{-1} in offshore (Fig. 3d). Surface chlorophyll patches (~0.3 μg L^{-1}) found between the offshore pelagic zone and the water-intrusion zone during the transect study (Fig. 3c) resulted from a surface phytoplankton bloom spreading from the southwest coast of Taiwan to the offshore regions of the central northern SCS (Fig. 2c).

Phytoplankton chlorophyll-*a* was generally vertically well mixed in the coastal ocean zone, with clear subsurface maxima of chlorophyll-*a* only found in the offshore pelagic zone and the water-intrusion zone (Fig. 3c). The depth of the subsurface chlorophyll maxima followed the σ_θ = 23.5 isopycnal, which became much shallower when

approaching the continental shelf from offshore. The vertical distribution of nutrients along the section generally followed the isopycnal surfaces in the upper water column (Fig. 3d-f), revealing the importance of physical control on upper ocean biogeochemistry. The observed uplift of isopycnals as well as the depths of chlorophyll maximum and nutricline at the shelf station C_6 and the offshore station C_{12} were consistent with positive upwelling velocities driven by wind stress curl (Fig. 2b). Interestingly, there were substantially higher nutrient concentrations and nutrient gradients at depths of ~200 m (across the σ_θ = 25.5 isopycnal) for both stations C_9 and C_{11} in the offshore regions, which could be due to either a horizontal or diapycnal injection event prior to our survey. Elevated chlorophyll-*a* found at station C_{11} was consistent with its high salinity in the euphotic zone and high nutrient concentrations below the euphotic zone, suggesting possible horizontal and vertical nutrient transports. Diapycnal fluxes would be more important than the horizontal fluxes in the offshore regions, as horizontal nutrient gradients within euphotic zone are considerably lower than the vertical gradient. Curiously, low chlorophyll-*a* was observed at station C_9, which had the highest nutrient concentrations and nutrient gradients. Along the density interval of σ_θ = 25 and σ_θ = 26 in the water-intrusion zone there was evidence for isopycnal mixing of the high-nutrient South China Sea waters with adjacent waters from Luzon Strait with much lower nutrient, but higher temperature/salinity, presumably from Pacific intermediate water.

3.3 Vertical diffusivity and diffusive nutrient fluxes

Turbulent diffusivity estimated from Thorpe analyses during the survey of May 2014 varied substantially from the edge of continental shelf to the west of Luzon Strait (Fig. 4) with an average K_z of 2.5×10^{-4} m^2 s^{-1} in the upper 300 m for the offshore deep-water stations. This is much higher than the oceanic background diffusivity of 10^{-5} m^2 s^{-1} but is comparable with previous basin-scale estimates from the northeastern SCS (Tian et al., 2009; Liu and Lozovatsky 2012). There were relatively high mean diffusivities of 3.6×10^{-4} and 3.3×10^{-4} m^2 s^{-1} at stations C_8 and C_{11}, respectively, but an order of magnitude lower diffusivity of 2.5×10^{-5} m^2 s^{-1} at station C_9. The estimated diffusive nitrate flux at the base of euphotic zone was only ~0.26 mmol m^{-2} d^{-1} for station C_9, substantially lower than the ~1.7 mmol m^{-2} d^{-1} of station C_{11}, even though the nitrate

gradient for C_9 (0.12 mmol m^{-2}) was about twice of that of C_{11} (0.06 mmol m^{-2}). The elevated Thorpe scales and diffusivities at stations C_8 and C_{11} were consistent with their high chlorophyll-*a* concentrations: the diffusive nutrients from below would expected to support higher euphotic zone phytoplankton production. Our data also revealed a general decrease of mean diffusivity from 1.1×10^{-3} m^2 s^{-1} at station C_5 on the continental shelf, to 6.3×10^{-4} m^2 s^{-1} of station C_6 over the continental slope, and to 9.1×10^{-5} m^2 s^{-1} at station C_7 in the offshore pelagic regions. These estimates of turbulent diffusivity from the continental shelf to offshore were in good agreement with previous microstructure measurements from the northeastern SCS. Yang et al., (2014) measured the eddy diffusivity due to turbulent kinetic energy dissipation using a microstructure profiler along a short section near the edge of the continental shelf southwest of Taiwan during May 2004 – about the same place as our stations C_5 to C_7 (Fig. 1). Their results showed high turbulent mixing over the continental shelf with a mean diffusivity of 1.6×10^{-3} m^2 s^{-1} but a much lower diffusivity of 5.2×10^{-4} m^2 s^{-1} over the slope (Yang et al., 2014).

The vertical structure of diffusivity was quite patchy due to the intermittent nature of turbulence dissipation (Fig. 4 and Fig. 5). Turbulent diffusivities at the two incubation stations (stations A and B) were compared to those of a time-series reference station S_1 (Fig. 5), which had been continuously sampled with up to 13 CTD casts over 24 hours, thus providing better vertical resolution of diffusivity for the study area. The pattern of diffusivity in station A showed a good agreement with that at the reference station S_1 (Fig. 5), as the stations were very close to each other (Fig. 1). However, there was much higher diffusivities found at station B compared to station S_1 (Fig. 5), which could be attributed to wave-induced turbulence southeast of Dongsha Island. It had been suggested that the internal tides propagating westward from the Luzon Strait would produce high-frequency internal waves over the shoaling bathymetry east of Dongsha Island, leading to diapycnal diffusivity on the order of 10^{-3} m^2 s^{-1} during April 2000 (Lien et al., 2005). The average diffusivity at 100 m during our field study was about 1.6×10^{-4} m^2 s^{-1} for station A but about 4.4×10^{-4} m^2 s^{-1} for station B. The corresponding diffusive nitrate fluxes at the base of euphotic zone would thus be about 0.65 mmol m^{-2} d^{-1} for station A and 3.03 mmol m^{-2} d^{-1} for station B, given their nitrate gradients of 0.05 and 0.08 mmol m^{-2} at 100 m, respectively (Table 1).

3.4 Phytoplankton growth and microzooplankton grazing

Two representative stations with one southwest of Taiwan (station A) and the other southeast of Dongsha Island (station B) were intensively studied with a comprehensive suite of measurements including both biogeochemical variables and phytoplankton growth and microzooplankton grazing rates. Station A was located at the edge of a surface phytoplankton bloom (Fig. 2c), which was spreading from the southwest coast of Taiwan to the offshore pelagic regions, while station B was close to the central northern SCS with very low sea surface chlorophyll-*a* (<0.1 μg L^{-1}). Except for the surface layer, chlorophyll-*a* concentrations at station B were generally much higher than that at station A throughout the water column. There was a clear subsurface chlorophyll maximum of ~0.4 μg L^{-1} at 50 m for station B (Fig. 6), while double peaks of chlorophyll-*a* were found for station A with a surface maximum of ~0.3 μg L^{-1} and a subsurface maximum of ~0.1 μg L^{-1} at 75 m. The hydrographic and biogeochemical conditions of these two stations were quite different, with much higher temperature (Fig. 6) and salinity (data not shown) but lower nutrients and nutrient gradients at station A than station B (Fig. 6). These results were consistent with previous reports (e.g., Chao et al., 1996), which suggested that the upper water column of the southwest Taiwan was influenced by the upwelled Pacific intermediate waters with generally high temperature and salinity but low nutrients after their penetration through the Luzon Strait into the SCS.

Rates of phytoplankton growth and microzooplankton grazing at the surface estimated from dilution experiments were substantially different between the two stations. The nutrient-saturated phytoplankton growth rate was 1.24 d^{-1} at station B, which was about three times of that at station A (0.44 d^{-1}). On the other hand, the microzooplankton grazing rate of 0.43 d^{-1} at station A was only slightly lower than the grazing rate of 0.60 d^{-1} at station B (Fig. 7). The natural growth rate of phytoplankton, after correction for the effects of nutrient enrichment as described in section 2.3, was 0.28 d^{-1} at station A, much lower than the rate of 1.18 d^{-1} in station B. The rates measured at station B during May 2014 were comparable with previous estimates of growth rates of 1.03 d^{-1} and grazing rates of 0.62 d^{-1} near Dongsha Island during July 2009 (Chen et al., 2013). Our results for station A were also in good agreement with those found in the non-upwelling area of the

south Taiwan Strait (Huang et al., 2011), which suggested mean rates of 0.4-0.5 d^{-1} and 0.3-0.7 d^{-1} for phytoplankton growth and microzooplankton grazing during July 2004 and 2005.

Nutrient-enriched incubations of phytoplankton at station A indicated that phytoplankton chlorophyll-*a* showed an exponential growth response within the first two days before reaching a stable growth phase on the third day and a decay phase on the fourth day; the chlorophyll-*a* of the control experiment with raw seawater without nutrient additions quickly decreased as nutrients were consumed in the bottles (Fig. 8a). In contrast, phytoplankton of station B showed no response to nutrient enrichment within the first two days of incubation compared to the control experiment (Fig. 8b). Significant increase of incubated phytoplankton chlorophyll-*a* for station B was only found during the last two days of incubation (Fig. 8b). Nutrient utilization during nutrient-enrichment incubations at these two stations were also quite different, with a much slower specific rate of nutrient consumption at station B (0.46 d^{-1}) than at station A (1.03 d^{-1}). These results suggest that there was stronger nutrient limitation of the phytoplankton community at station A than station B.

4. Discussion

4. 1 Roles of turbulent mixing and curl-driven upwelling on nutrient fluxes of the northeastern SCS during the spring inter-monsoon transition period

If the horizontal and atmospheric inputs are ignored, the vertical nutrient flux into the euphotic zone (J_{total}) should be the sum of diffusive flux due to turbulent dissipation ($J_{dif}=K_z\partial C/\partial z$) and the advective flux due to upwelling ($J_{upw}=wC$, negative for downwelling):

$$J_{total} = K_z \frac{\partial C}{\partial z} + wC \quad (6)$$

To compare the roles of turbulent diffusion and Ekman pumping on vertical transport of nutrients in the northeastern SCS, we estimated the diffusive and advective nitrate fluxes at the base of euphotic zone from the continental shelf to the open sea during May 2014 (see Table 1 for details). The vertical velocity (w) at the based of euphotic zone was

assumed equal to the Ekman velocity (w_e) to estimate the upwelling fluxes. Here, we have focused on Ekman pumping by neglecting Ekman transport as its effect was restricted only to the near coast (Gan et al., 2010). Variations of Ekman velocity by curl-driven upwelling/downwelling during the transect study is consistent with isopycnal oscillations observed at depth along the section (Fig. 3), suggesting the important role of Ekman pumping on the physical dynamics of the water column. At the continental slope station C_6, vertical nitrate fluxes were largely supported by curl-driven upwelling, with turbulent mixing playing a minor role due to its low nitrate gradient. In contrast, the diffusive nitrate flux was more than three times the upwelled nitrate flux at station C_7, immediately adjacent to station C_6. Except at station C_{12}, curl-driven downwelling was generally observed at the offshore pelagic stations during the 3-day transect study, which resulted in downward transport of low-nutrient surface water into the deeper layer. Therefore, the upward fluxes of nitrate into the euphotic zone for these stations were determined by the intensities of diffusive fluxes working against the downwelling fluxes. There was a negative nitrate flux found at station C_9 where downwelling was stronger than the upward diffusion, resulting in a loss of nitrate from the euphotic zone. Our findings suggest that it is the interplay of turbulent diffusion and curl-driven upwelling/downwelling that controls the vertical fluxes of nutrients into the euphotic zone to support phytoplankton production in the northeastern SCS.

The integrated phytoplankton chlorophyll-*a* biomass during the transect study showed a positive correlation with upward nitrate flux ($\int Chl \cdot dz = 12.9 \times J_{total} + 10$, $r^2 = 0.35$) when station C_9 was not included (Table 1), supporting the important role of bottom-up control on phytoplankton production in our study area (Chen 2005). From the slope of 12.9, we can estimate a specific new production by vertical nitrate supply of 0.078 molN $(gChl)^{-1}$ d^{-1}, which is well within the range of 0.063-0.088 molN $(gChl)^{-1}$ d^{-1} reported in the northern SCS by Chen (2005). The largest diffusive nitrate flux found at station B, with an enhanced vertical diffusivity and steeper nutrient gradient, could be attributed to strong vertical shear and large dissipation induced by nonlinear internal waves that are generated at the edge of the continental shelf near Dongsha Island (Lien et al., 2005). This wave-induced turbulent mixing was related to enhanced surface chlorophyll-*a* and net primary production near Dongsha Island compared to adjacent areas with minimal

influence of internal waves during the summertime (Pan et al., 2012). Assuming a vertically constant rate of phytoplankton specific growth, a gram chlorophyll-to-carbon ratio of 0.03 and a molar C/N ratio of 6.625, we estimated a vertically integrated primary production of ~12.3 mmolN m^{-2} d^{-1} in station B and ~1.8 mmolN m^{-2} d^{-1} in station A. The contribution of vertical nutrient fluxes to primary production would thus be ~11% and ~26% in stations B and A, respectively, which are comparable with the *f*-ratio of 0.14-0.20 previously estimated in the northern SCS from late March to October (Chen, 2005). In steady status, the net primary production of phytoplankton should be balanced by the upward nutrient flux as well as the downward particle flux. Therefore, a high nutrient flux would correspond to a high net primary production and thus a high biomass accumulation, if other conditions remain the same (species, temperature, light, grazing, etc). Station C_9 is interesting in that the vertical nutrient fluxes are net downward out of euphotic zone, suggesting that the station might not be in steady status. High nutrients here were likely a result of strong horizontal input or a previous diapycnal nutrient injection. In this case, large drawdown of nutrients would be expected by fast growing phytoplankton and by the downward transport of nutrients out of euphotic zone.

Uncertainty of vertical nutrient fluxes including diffusive and advective fluxes could be contributed by errors in the determinations of vertical diffusivity and vertical velocity, as well as nutrient concentration and gradient. Calculation errors of vertical diffusivity by the Thorpe-scale approach, estimated from a time-series station S_1 with continuous sampling up to 13 casts in 24 hours, were 0.87 x10^{-4} m^{-2} s^{-1} at 50 m (n=5), 0.71 x10^{-4} m^{-2} s^{-1} at 100 m (n=6), and 0.46 x10^{-4} m^{-2} s^{-1} at 150 m (n=7). We could therefore obtain an average of 0.68 x10^{-4} m^{-2} s^{-1} for the overall uncertainty of diffusivity determined in our study. Uncertainty of vertical velocity by Ekman pumping from satellite observations could be approximately determined at each station by their standard deviations over the sampling duration of May 14th-16th, 2014. Measurement errors of nutrients at depths during the field study could be negligible as the concentrations are considerably higher than the detection limits of the analytical methods (Li and Hansell, 2008). We are not able to quantify the uncertainty of nutrient gradient, as we have only one cast for each station with reduced resolution below the euphotic layer. Meanwhile, the nutrient gradient and related diffusive flux that we have calculated at the base of euphotic zone

could be interpreted as a mean value between the two adjacent bottle depths (100-200 m). The final uncertainties for the vertical nutrient fluxes are summarized in Table 1, which vary substantially from 0.10 to 0.98 mmol m^{-2} d^{-1} for stations in the offshore regions.

4.2 Impact of growth-grazing dynamics on phytoplankton chlorophyll biomass in the northeastern South China Sea

Distributions of phytoplankton in the ocean are controlled by complex physical and biological interactions. To study the influence of growth-grazing dynamics on phytoplankton chlorophyll-*a* biomass in the northern SCS, two stations with distinct biogeochemical settings and nutrient fluxes were selected for measurements of phytoplankton growth and microzooplankton grazing rates. In addition, the community response to nutrient enrichments at the two stations was assessed by continuous incubations for up to four days. Substantially high phytoplankton growth rates observed at station B southeast of Dongsha Island was in agreement with its high nutrient concentrations and nutrient fluxes compared to station A south of Taiwan Strait. When released from the constraints of nutrient limitation, the phytoplankton community would be expected to shift from dominance by picoplankton toward a higher relative abundance of larger phytoplankton such as diatoms, with their higher intrinsic capacity for growth (Agawin et al., 2000). In fact, through phytoplankton pigment analyses higher diatom abundance was observed at station B than station A, which was consistent with previous reports that surface phytoplankton community in the southeast Dongsha Island was dominated by both diatom and picoplankton such as *Prochlorococcus*, while picoplankton with negligible diatoms were found in the non-upwelling area south of the Taiwan Strait near station A during late spring and early summer (Yang 2009; Huang et al., 2011).

The ratio of the microzooplankton grazing rate to the phytoplankton growth rate (g/μ) represents the percentage of the primary production consumed by microzooplankton (Landry et al., 1998). High g/μ ratios (~1.5) at station A suggest an elevated role of the microbial food web in the south Taiwan Strait, promoting nutrient recycling that could support further phytoplankton growth. Whereas, the relatively higher microzooplankton grazing rate but lower g/μ ratio at station B may indicate a greater efficiency of carbon

export near the Dongsha Island, as the loss of diatoms through sinking or grazing by mesozooplankton in regions with high nutrient supply (Landry et al., 1998). The natural growth rate of phytoplankton at station B was much higher than the grazing mortality rate, leading to a large net growth rate (growth minus grazing) of 0.58 d^{-1}, which is consistent with the higher integrated chlorophyll biomass at station B. A negative net growth rate of -0.15 d^{-1} was found at station A. The specific phosphate consumption rate of 1.03 d^{-1} at station A was about twice of that of 0.46 d^{-1} at station B suggesting a larger nutrient demand at station A. There was actually a faster response of phytoplankton chlorophyll-*a* to nutrient enrichment at station A than at station B indicating the potential for stronger nutrient limitation of the phytoplankton community in the south Taiwan Strait. The negative net community growth and the higher nutrient consumption rate at station A are consistent with the spring phytoplankton bloom of the southwest Taiwan observed in the satellite data (Fig. 2c) being in its decline phase. Indeed, the area of the phytoplankton bloom decreased substantially within two weeks and was not visible by the middle of June, 2014 (from weekly mean sea surface chlorophyll-*a* data of MODIS Aqua) supporting the important role of grazing activity on phytoplankton distribution in the northern SCS.

In conclusion, we have conducted a preliminary study on vertical nutrient fluxes and phytoplankton dynamics in the northeastern SCS. Our results suggest that phytoplankton patchiness in the northeastern SCS during the spring inter-monsoon of May 2014 was mainly controlled by vertical nutrient fluxes, which were driven by both turbulent diffusion and wind stress curl-driven upwelling. Our results also revealed an increasing role of turbulent diffusion but a decreasing role of curl-driven upwelling on vertical transport of nutrients from the coastal ocean zones to the offshore pelagic zones in the northeastern SCS. Elevated nutrient fluxes observed near the Dongsha Island were found to support high new production leading to net growth of a diatom-rich phytoplankton community, whereas the low nutrient fluxes of the south Taiwan Strait resulted in a negative net community growth leading to a decline of a picoplankton-dominant phytoplankton bloom. As the findings presented here is limited by the very narrow area and the very short period of sampling time, future studies may be improved by addressing the variability of vertical nutrient fluxes and its relationship to phytoplankton dynamics

552 on a much longer time scale over a much broader area of the northern SCS.

553

554 *Acknowledgements*

555 We are grateful to the captain and crew of the *R/V Shiyan III* for their helps during the
556 field work. This work is supported by a startup fund from a National Talent-Recruitment
557 Program and a grant from the Chinese Academy of Sciences' Strategic Pilot Project
558 No.XDA110202014 (to QPL).

559 *References*

560 Abraham, E.R.: The generation of plankton patchiness by turbulent stirring, Nature, 391,
561 577-580, 1998.
562 Agawin, N.S.R., Duarte, C.M., and Agusti, S.: Nutrient and temperature control of the
563 contribution of picoplankton to phytoplankton biomass and production, Limnol. Oceanogr., 45,
564 591-600, 2000.
565 Bombar, D., Dippner, J.W., Doan, H.N., Ngoc, L.N., Liskow, I., Loick-Wilde, N., and Voss,
566 M.: Sources of new nitrogen in the Vietnamese upwelling region of the South China Sea, J.
567 Geophys. Res., 115, C06018, doi:10.1029/2008JC005154, 2010.
568 Centurioni, L.R., Niiler, P.P., and Lee, D.K.: Observations of inflow of Philippine Sea surface
569 water into the South China Sea through the Luzon Strait, J. Phys. Oceanogr., 34, 113-121, 2004.
570 Chao, S.Y., Shaw, P.T., and Wu, S.Y.: Deep water ventilation in the South China Sea,
571 Deep-Sea Res., I 43, 445-466, 1996.
572 Chen, B., Liu, H., Landry, M.R., Dai, M., Huang, B., and Sun, J.: Close coupling between
573 phytoplankton growth and microzooplankton grazing in the western South China Sea, Limnol.
574 Oceanogr., 54, 1084-1097, 2009.
575 Chen, B., Zheng, L., Huang, B., Song, S., and Liu, H.: Seasonal and spatial comparisons of
576 phytoplankton growth and mortality rates due to microzooplankton grazing in the northern South
577 China Sea, Biogeosciences, 10, 2775-2785, 2013.
578 Chen, Y.L.: Spatial and seasonal variations of nitrate-based new production and primary
579 production in the South China Sea, Deep-Sea Res., II, 52, 319-340, 2005
580 Cullen, J.J., Franks, P.J.S., Karl, D.M., and Longhurst, A.: Physical influences on marine
581 ecosystem dynamics, in: The sea, 12, Robinson, A.R., McCarthy, J.J., Rothschild, B.J. (eds), John
582 Wiley & Sons, New York, 297–336, 2002.
583 Davis, C.S., Flierl, G.R., Wiebe, P.H., and Franks, P.J.S.: Micropatchiness, turbulence and
584 recruitment in plankton, J. Mar. Res., 43, 109-151, 1991.
585 Eppley, R.W., and Peterson, B.J.: Particulate organic matter flux and planktonic new
586 production in the deep ocean, Nature, 282, 677-680,1979.
587 Farris, A., and Wimbush, M.: Wind-induced intrusion into the South China Sea, J. Oceanogr.,
588 52, 771–784, 1996.
589 Galbraith, P.S., and Kelley, D.E.: Identifying Overturns in CTD Profiles, J. Atmos. Ocean.
590 Tech., 13, 688–702, 1996.
591 Gan, J., Lu, Z., Dai, M., Cheung, A., Liu, H., and Harrison, P.: Biological response to
592 intensified upwelling and to a river plume in the northeastern South China Sea: A modeling study,

J. Geophys. Res., 115, doi: 10.1029/2009jc005569, 2010.

Gargett, A. E., and Garner, T.: Determining Thorpe scales from ship-lowered CTD density profiles, J. Atmos. Ocean. Tech., 25, 1657–1670, 2008.

Gaube, P., Chelton, D.B., Strutton, P.G., and Behrenfeld, M.J.: Satellite observations of chlorophyll, phytoplankton biomass, and Ekman pumping in nonlinear mesoscale eddies, J. Geophys. Res., 118, 6349-6370, doi:10.1002/2013JC009027, 2013.

Gill, A.E. (Eds.): Atmosphere-Ocean Dynamics, International Geophysics Series, 30, Academic Press, London, 1982.

Han, A., Dai, M., Gan, J., Kao, S., Zhao, X., Jan, S., Li, Q., Lin, H., Chen, C., Wang, L., Hu, J. Wang, L., and Gong. F.: Inter-shelf nutrient transport from the East China Sea as a major nutrient source supporting winter primary production on the northeaster South China Sea shelf, Biogeosciences, 10, 8159-8170, 2013.

Huang, B., Xiang, W., Zeng, X., Chiang, K., Tian, H., Hu, J., Lan, W., and Hong. H.: Phytoplankton growth and microzooplankton grazing in a subtropical coastal upwelling system in the Taiwan Strait, Cont. Shelf Res, 31, 48-56, 2011.

Kim, T.K., Lee, K., Duce, R., Liss, P.: Impact of atmospheric nitrogen deposition on phytoplankton productivity in the South China Sea, Geophys. Res. Letters, 41(9), 3156-3162, 2013.

Landry, M.R., Brown, S.L., Campbell, L., Constantinou, J., and Liu, B.: Spatial patterns in phytoplankton growth and microzooplankton grazing in the Arabian Sea during monsoon forcing, Deep-Sea Res., II, 45, 2353-2368, 1998.

Landry, M.R., and Hassett, R. P.: Estimating the grazing impact of marine micro-zooplankton, Mar. Biol., 67(3), 283-288, 1982.

Li, Q.P., Franks, P.J.S., and Landry, M.R.: Microzooplankton grazing dynamics: parameterizing grazing models with dilution experiment data in the California Current Ecosystem, Mar. Ecol. Prog. Ser., 438, 59-69, 2011.

Li, Q.P., Franks, P.J.S., Ohman, M.D., and Landry, M.R.: Enhanced nitrate flux and biological processes in a frontal zone of the California Current System, J. Plankton Res., 34, 790-801, 2012.

Li, Q.P., and Hansell, D.A.: Nutrient distribution in baroclinic eddies of the oligotrophic North Atlantic and inferred impacts on biology, Deep-Sea Res., II, 55, 1291-1299, 2008.

Lien, R., Tang, T., Chang, M., and D'Asaro, E.A.: Energy of nonlinear internal waves in the South China Sea, Geophys. Res. Lett., 32, L05615, doi:10.1029/2004GL022012, 2005.

Lin, I., Lien, C., Wu, C., Wong, G.T.F., Huang, C., and Chiang, T.: Enhanced primary production in the oligotrophic South China Sea by eddy injection in spring, Geophys. Res. Letters,

627 37, L16602, doi:10.1029/2010GL043872, 2010.
628 Lin, I., Wong, G.T.F., Lien, C., Chien, C., Huang, C., and Chen, J.: Aerosol impact on the
629 South China Sea biogeochemistry: an early assessment from remote sensing, Geophys. Res.
630 Letters, 36, L17605, doi:10.1029/2009GL037484, 2009.
631 Liu, K.K., Chao, S.Y., Shaw, P.T., Gong, G.C., Chen, C.C., and Tang, T.Y.: Monsoon-forced
632 chlorophyll distribution and primary production in the South China Sea: observations and a
633 numerical study, Deep-Sea Res., I, 49, 1387-1412, 2002.
634 Liu, X., Furuya, K., Shiozaki, T., Masuda, T., Kodama, T.. Sato, M.. Kaneko, H.. Nagasawa,
635 M.. and Yasuda, I.: Variability in nitrogen sources for new production in the vicinity of the shelf
636 edge of the East China Sea in summer, Cont., Shelf Res., 61-62, 23-30, 2013.
637 Liu, Z.Y., and Lozovatsky, I.: Upper pycnocline turbulence in the northern South China Sea,
638 Chin. Sci. Bull., 57(18), 2302-2306, 2012.
639 Mahadevan, A., and Tandon, A.: An analysis of mechanisms for submesoscale vertical motion
640 at ocean fronts, Ocean Modelling, 14, 241-256, 2006.
641 Osborn, T.R.: Estimates of the local rate of vertical diffusion from dissipation measurements,
642 J. Phys. Oceanogr., 10(1), 83-89, 1980.
643 Pan, X., Wong, G.T.F., Shiah, F.K., and Ho. T.Y.: Enhancement of biological production by
644 internal waves: observations in the summertime in the northern South China Sea, J. Oceanogr., 68,
645 427-437, 2012.
646 Parsons, T.R., Maita, Y., and Lalli, C.M. (Eds.): A manual of chemical and biological methods
647 for seawater analysis, Pergamum Press, Oxford, 1984.
648 Risien, C.M., and Chelton, D.B.: A global climatology of surface wind and wind stress fields
649 from eight year QuickSCAT scatterometer data, J. Phys. Oceanogr., 38, 2379-2412, 2008.
650 Rykaczewski, R.R., and Checkley, D.M.: Influence of ocean winds on the pelagic ecosystem
651 in upwelling regions, PNAS, 105(6), 1065–1970, 2008.
652 Strom, S. L., Macri, E. L., and Olson, M. B.: Microzooplankton grazing in the coastal Gulf of
653 Alaska: Variations in top-down control of phytoplankton, Limnol. Oceanogr., 52, 1480–1494,
654 2007.
655 Tian, J., Yang, Q., and Zhao, W.: Enhanced diapycnal mixing in the South China Sea. J. Phys.
656 Oceanogr., 39, 3191-3203, 2009.
657 Thorpe, S.A.: Turbulence and mixing in a Scottish loch, Phil. Trans. Royal Soc., London A,
658 286, 125–181, 1977.
659 Wang, J., and Tang, D.: Phytoplankton patchiness during spring intermonsoon in west coast
660 of South China Sea, Deep-Sea Res, II, 101, 120-128, 2014.

Yang, Q., Tian, J., Zhao, W., Liang, X., and Zhou, L.: Observations of turbulence on the shelf and slope of northern South China Sea, Deep-Sea Res., I, 87, 43-52, 2014.

Yang, Y.H.: Phytoplankton community structure of the northern South China Sea and the Philippine Sea, Master Thesis (in CHN), National Taiwan Normal University, Taiwan, 73 pp., 2009.

Zhou, L., Tan, Y., Huang, L., Huang, J., Liu, H., and Lian, X.: Phytoplankton growth and microzooplankton grazing in the continental shelf area of northeastern South China Sea after typhoon Fengshen, Cont. Shelf Res., 31, 1663-1671, 2011.

669 Table 1: Comparisons of integrated chlorophyll-*a* ($\int Chl \cdot dz$), nitrate gradient ($\partial C/\partial z$), nitrate
670 concentration (NO_3), vertical diffusivity (K_z), upwelling velocity (w_e), diffusive nitrate flux
671 (J_{dif}), upwelled nitrate flux (J_{upw}), and total nitrate flux (J_{total}) for transect stations $C_{6\text{-}12}$ and
672 incubation stations A and B at ~1% light depth (~100m depth).

Station	$\int Chl \cdot dz$ [mg m^{-2}]	$\partial C/\partial z$ [mmol m^{-4}]	NO_3 [mmol m^{-3}]	[a] K_z [10^{-4} m^2 s^{-1}]	[b] w_e [10^{-5} m s^{-1}]	J_{dif} [mmol m^{-2} d^{-1}]	[c] J_{upw} [mmol m^{-2} d^{-1}]	J_{total} [mmol m^{-2} d^{-1}]
C_6	16.8	0.001	5.01	6.30±0.68	0.28±0.02	0.05±0.01	1.21±0.09	1.27±0.10
C_7	20.2	0.077	6.42	0.91±0.68	0.03±0.05	0.60±0.45	0.17±0.27	0.77±0.73
C_8	22.1	0.079	7.47	3.60±0.68	-0.21±0.08	2.44±0.46	-1.36±0.52	1.09±0.98
C_9	15.4	0.122	9.52	0.25±0.68	-0.12±0.03	0.26±0.72	-0.99±0.25	-0.72±0.96
C_{10}	21.7	0.082	9.37	3.45±0.68	-0.18±0.03	2.44±0.48	-1.46±0.24	0.99±0.72
C_{11}	38.7	0.060	2.08	3.30±0.68	-0.27±0.07	1.71±0.35	-0.49±0.13	1.23±0.48
C_{12}	20.7	0.029	3.93	1.53±0.68	0.05±0.05	0.39±0.17	0.17±0.17	0.56±0.34
C_{13}	13.2	0.046	1.98	2.26±0.68	-0.27±0.17	0.91±0.27	-0.46±0.29	0.44±0.56
A	15.7	0.047	2.09	1.60±0.68	-0.09±0.04	0.65±0.28	-0.16±0.08	0.49±0.35
B	24.8	0.080	4.82	4.40±0.68	-0.41±0.11	3.03±0.47	-1.71±0.46	1.33±0.93

673

674 [a] uncertainty of K_z from Thorpe analyses is estimated as 0.68 $\times 10^{-4}$ m^2 s^{-1} (see text for detail)

675 [b] w_e are 3-day-mean of May 14th-16th, 2014, except station B that is of May 12th-14th, 2014

676 [c] assuming vertical velocity at the depth of 100m is equal to w_e.

Figure 1: Sampling map in the northeastern South China Sea during May 2014. Dash lines show the topography of the study area; solid dots are the stations for a transect study ($C_{1\text{-}13}$) during May 14^{th}-16^{th}, 2014; star is a time-series reference station (S_1); filled squares are two stations where shipboard dilution experiments were performed (A and B). Inserted plot shows the temperature/salinity diagram for the transect with arrows indicating waters from the coastal ocean zone (thick gray lines), the offshore pelagic zone (thick black lines), and the Kuroshio intrusion zone (thin lines).

Figure 2: Spatial distributions of (a) sea surface temperature, (b) curl-driven upwelling velocity, and (c) sea surface chlorophyll during the survey, together with (d) the time-series of curl-driven upwelling and wind stress at stations C_6 and C_{13} during May-June, 2014. Vectors in panel (a) and panel (b) are surface geostrophic currents and wind stresses, respectively; geostrophic current is from 3-day-mean altimetry data from NOAA/AOML; upwelling velocity and wind stress are from 3-day mean METOP-ASCAT data; sea surface temperature is 3-day-mean GOES-POES data; sea surface chlorophyll-*a* is monthly MODIS-Aqua data.

Figure 3: Vertical distributions of (a) temperature [T], (b) salinity [S], (c) chlorophyll-*a* [*Chl-a*], (d) nitrate [NO_3], (e) silicate [$Si(OH)_4$], and (f) phosphate [PO_4] along the coastal transect of the northern South China Sea. Overlaid white lines in each panel are isopycnals.

Figure 4: Profiles of Thorpe displacement (d_z), Thorpe scale (L_T), and turbulent diffusivity (K_z) for nine stations (C_5, C_6, C_7, C_8, C_9, C_{10}, C_{11}, C_{12}, C_{13}) from the edge of continental shelf to the west of Luzon Strait. Locations of these stations are shown in Figure 1.

Figure 5: Comparisons of vertical turbulent diffusivities (K_z) between two stations A and B. Black line is the result of the reference station S_1 with continuous CTD sampling up to 13 casts; circles are for station A (2 casts) with squares for station B (2 casts).

Figure 6: Comparisons of vertical profiles of chlorophyll-*a* [*Chl-a*], temperature [T], nutrients [$Si(OH)_4$, NO_3, PO_4], and nutrient gradients between two incubation stations A and B. Thick lines in each panel are for bottom axis with thin lines (open symbols) for top axis; dash lines are for station A with solid lines for station B.

Figure 7: Dilution experiment plots of phytoplankton net growth rates against the dilution factors for stations A and B. Filled circles are net growth rates of the raw seawater without nutrient enrichments.

Figure 8: Temporal variations of chlorophyll-*a* and phosphate during incubations with and without nutrient enrichments in stations A and B. Dash lines (filled symbols) are for chlorophyll-*a* in left axis with thin lines (open symbols) for phosphate in right axis; control is the incubation of raw seawater without nutrient addition.

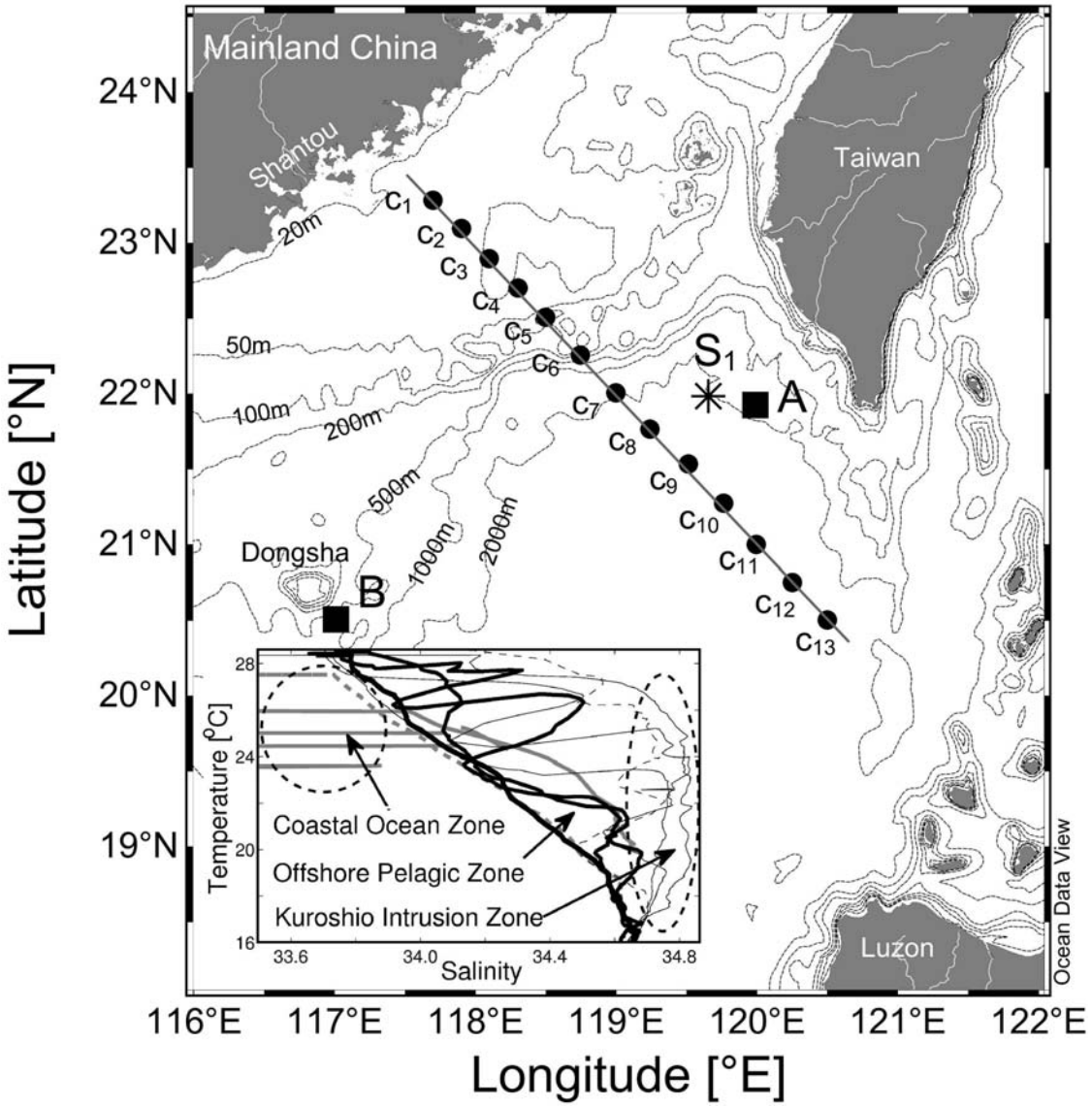

721
722
723 Figure 1

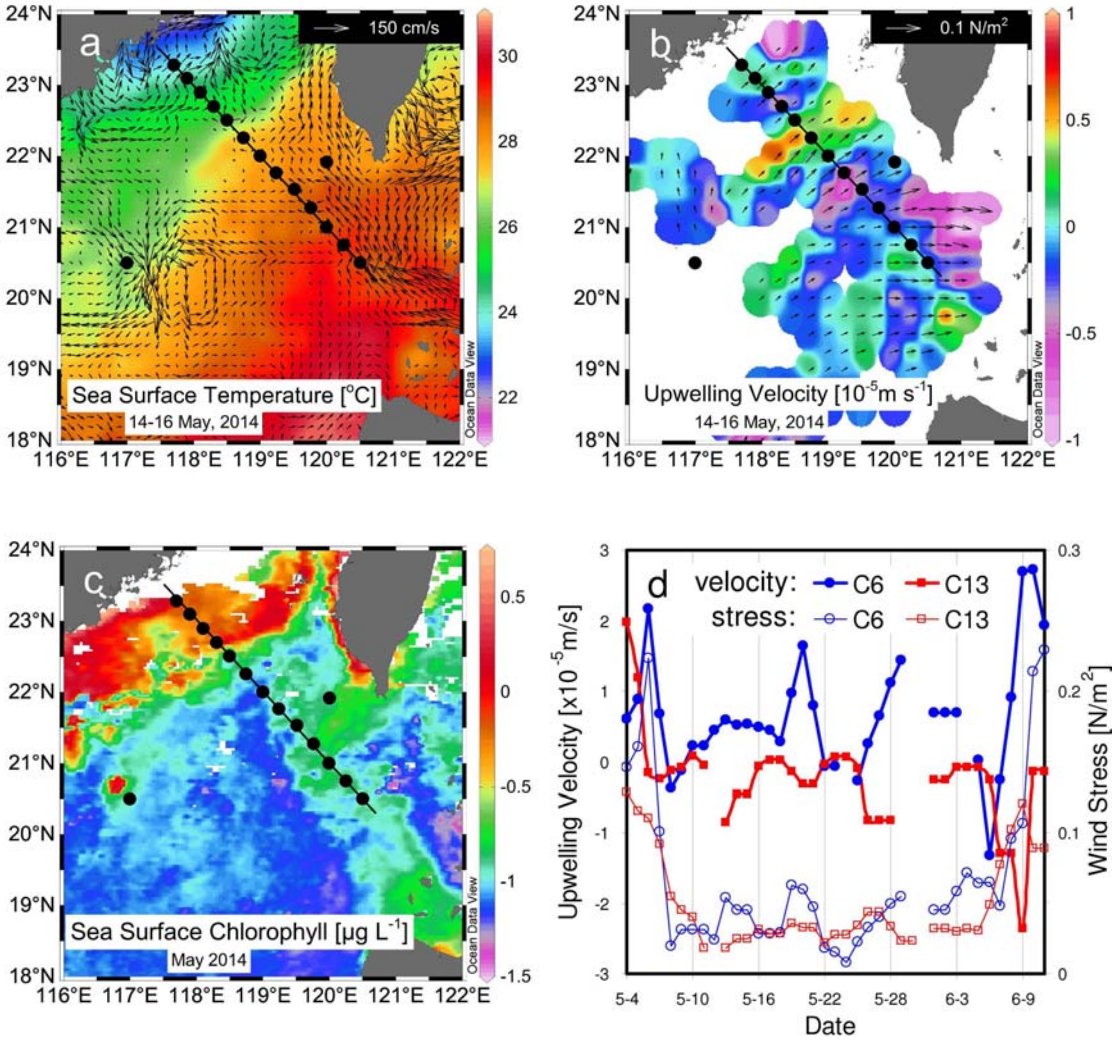
a
150 cm/s
Sea Surface Temperature [°C]
14-16 May, 2014
b
0.1 N/m²
Upwelling Velocity [10⁻⁵m s⁻¹]
14-16 May, 2014
c
Sea Surface Chlorophyll [μg L⁻¹]
May 2014
d
velocity: C6 C13
stress: C6 C13
Upwelling Velocity [x10⁻⁵m/s]
Wind Stress [N/m²]
Date
5-4
5-10
5-16
5-22
5-28
6-3
6-9
116°E 117°E 118°E 119°E 120°E 121°E 122°E
18°N 19°N 20°N 21°N 22°N 23°N 24°N

Figure 2

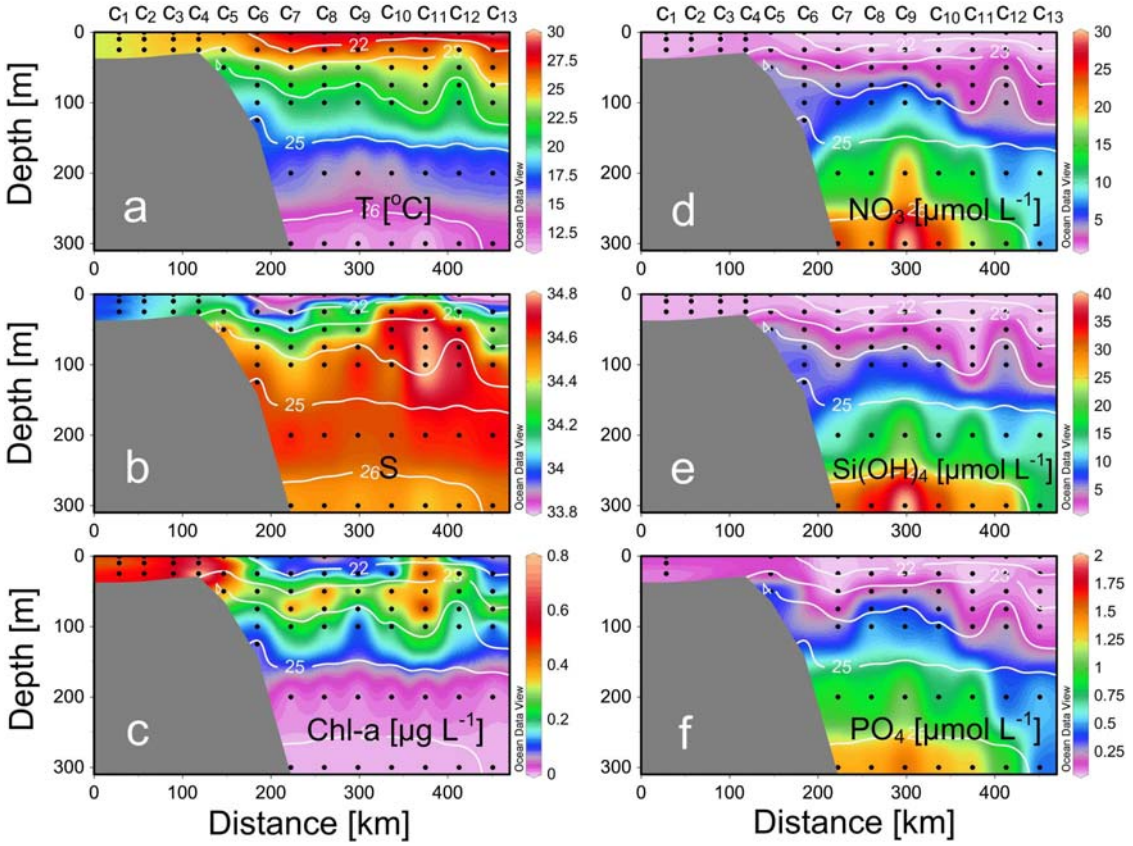
C1 C2 C3 C4 C5 C6 C7 C8 C9 C10 C11 C12 C13
Depth [m]
a
T [°C]
b
S
c
Chl-a [µg L-1]
d
NO3 [µmol L-1]
e
Si(OH)4 [µmol L-1]
f
PO4 [µmol L-1]
Distance [km]
Ocean Data View

Figure 3

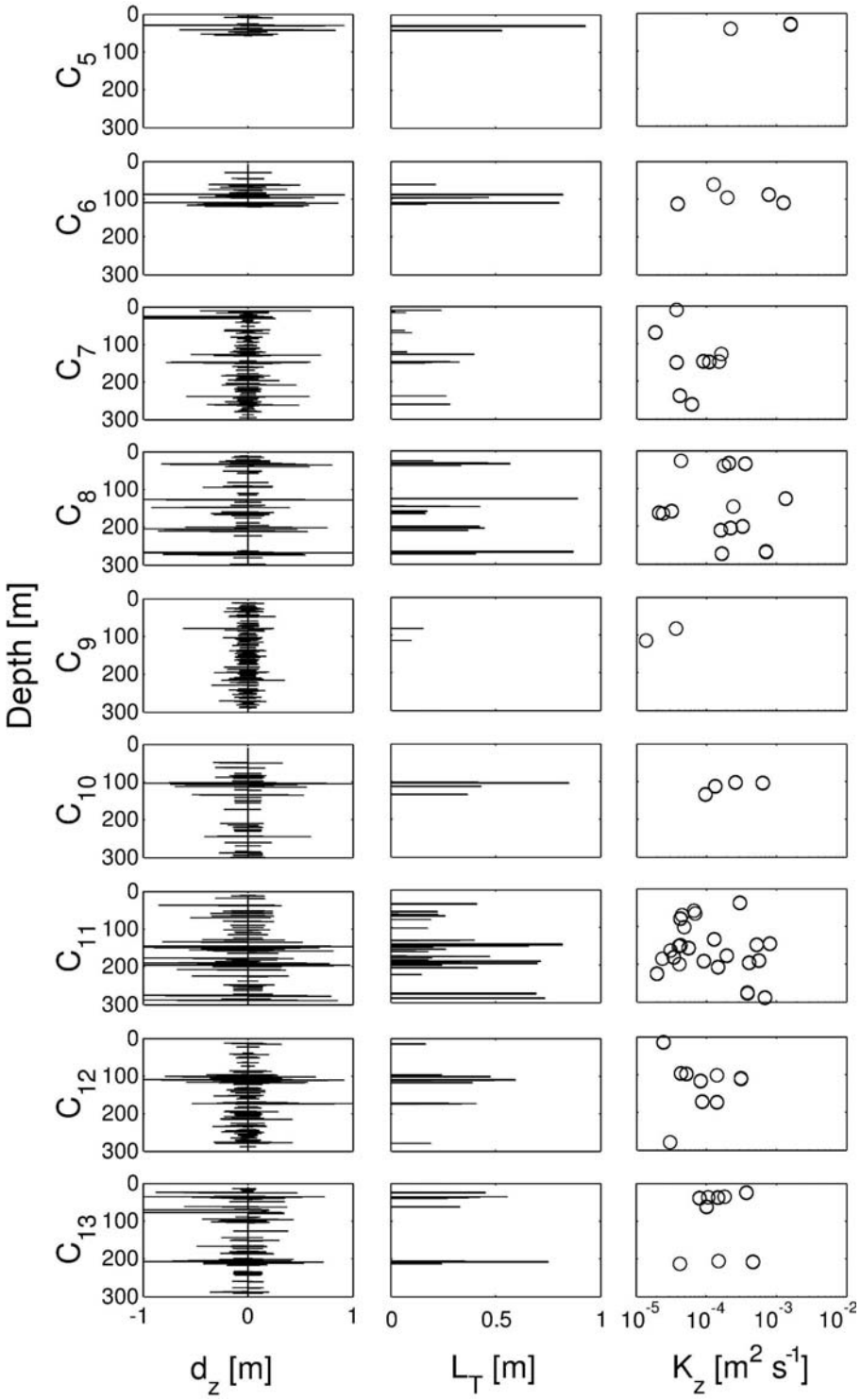

731
732
733 Figure 4

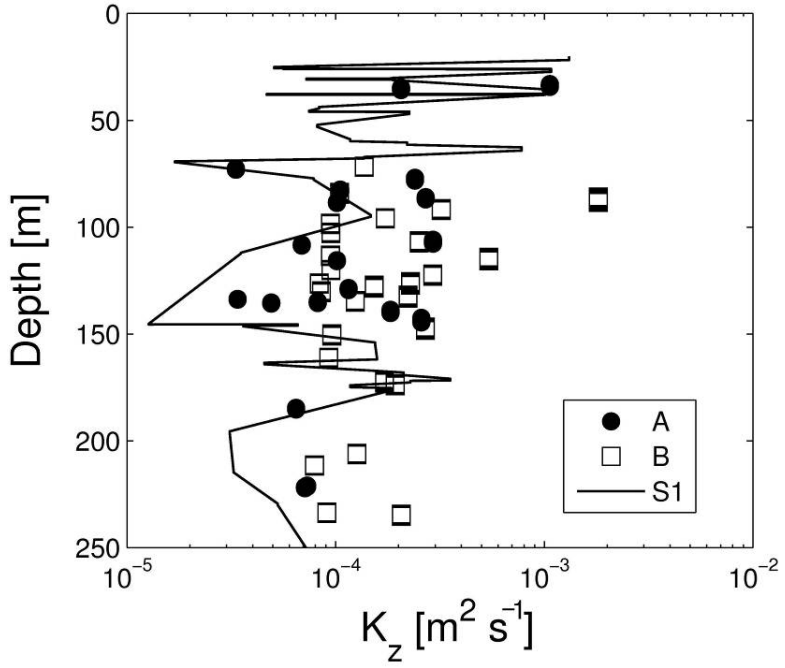

734
735
736 Figure 5

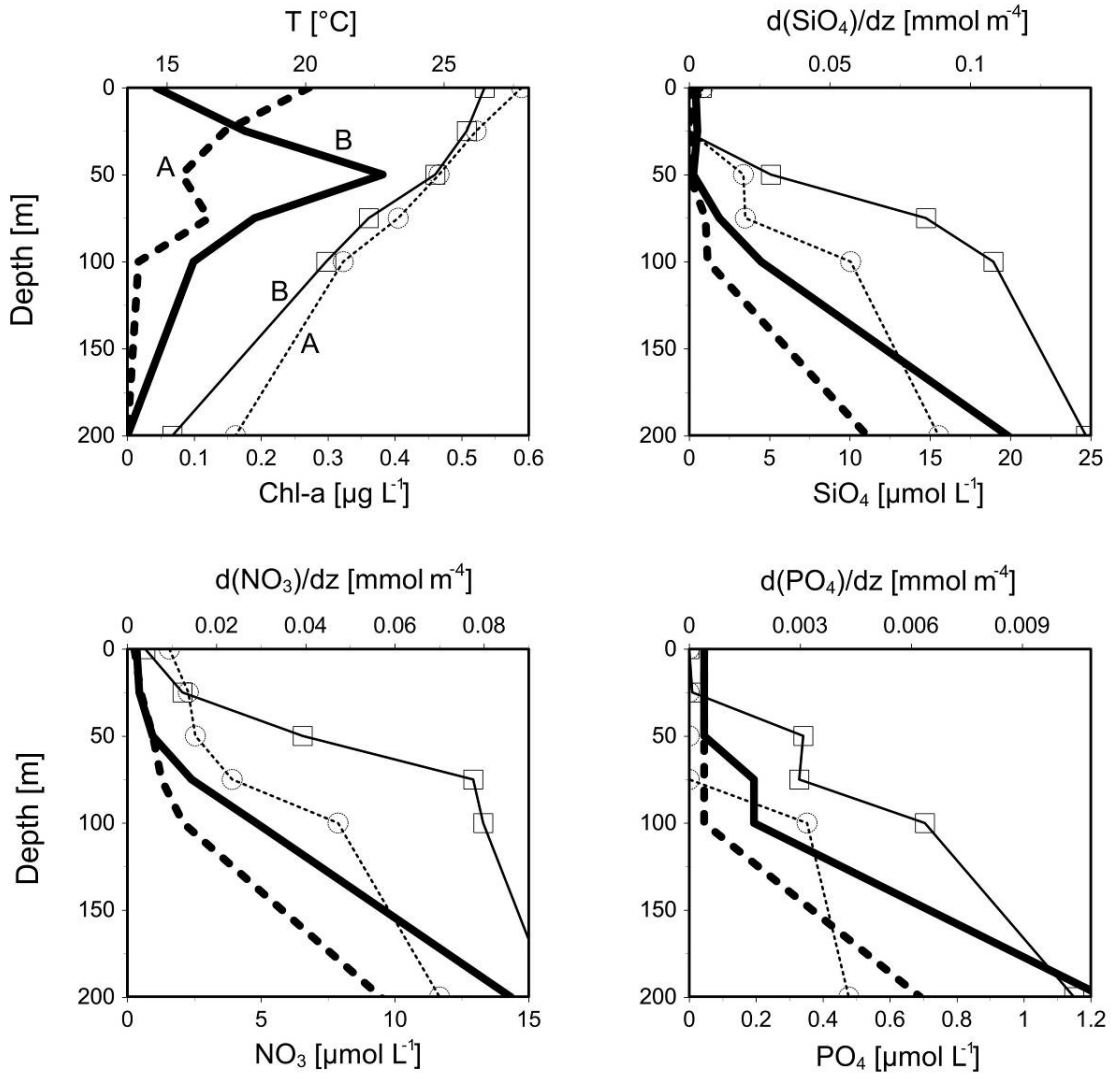

737
738
739 Figure 6

740

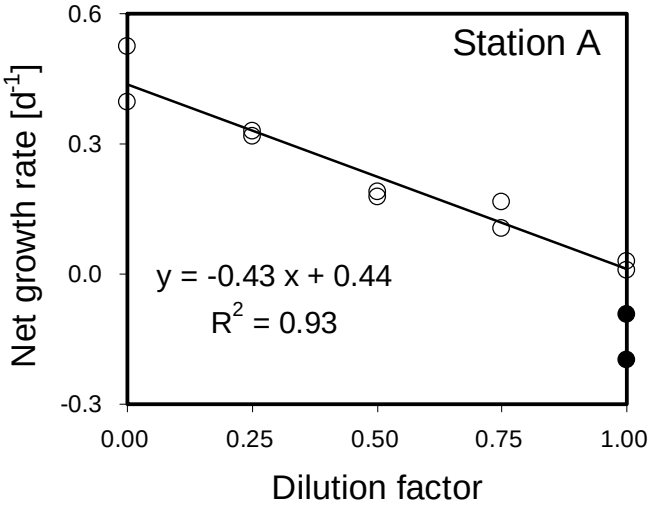

741

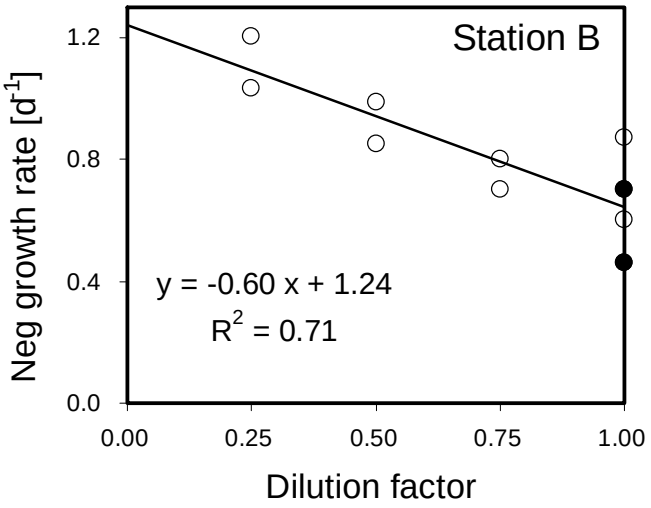

742
743
744 Figure 7

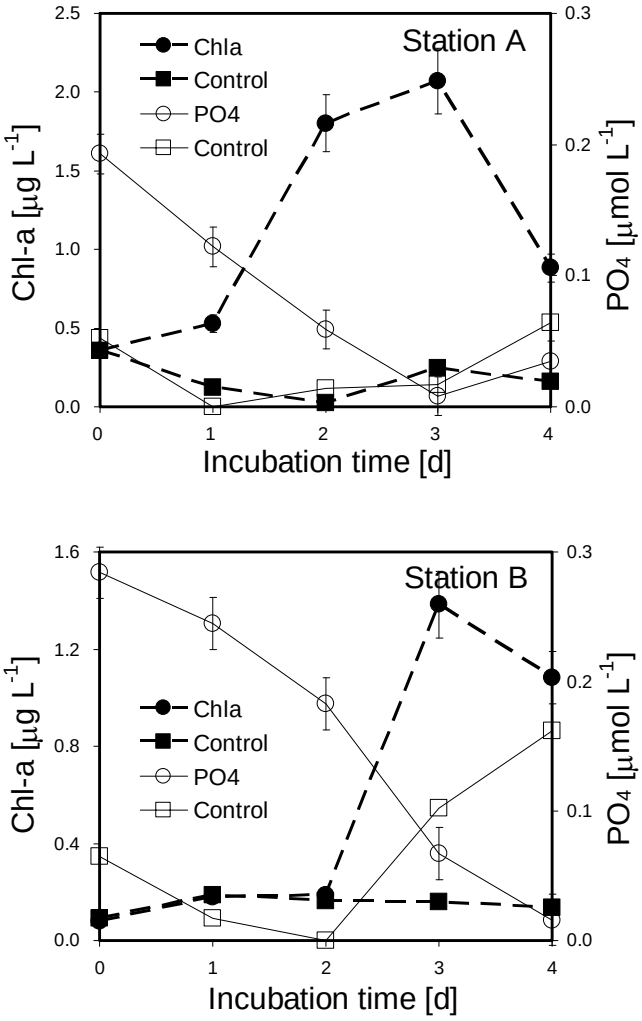
Station A
Chla
Control
PO4
Control
Chl-a [µg L-1]
PO4 [µmol L-1]
Incubation time [d]
Station B
Chla
Control
PO4
Control
Chl-a [µg L-1]
PO4 [µmol L-1]
Incubation time [d]

Figure 8